Spin-wave measurements on hexagonal MnTe of NiAs-type structure by inelastic neutron scattering

W. Szuszkiewicz,* E. Dynowska, and B. Witkowska
Institute of Physics, Polish Academy of Sciences, Al. Lotników 32/46, 02-668 Warsaw, Poland

B. Hennion
Laboratoire Léon Brillouin, CEA-CNRS, CE Saclay, 91191 Gif-sur-Yvette cedex, France
(Received 9 November 2005; revised manuscript received 11 January 2006; published 6 March 2006)

MnTe with a hexagonal structure of NiAs type is an antiferromagnetic semiconductor below the Néel temperature T_N=310 K. The spin-wave excitations of a MnTe single crystal have been measured at T=11 K by inelastic neutron scattering. The experimental spin-wave dispersions, obtained along five high-symmetry directions of the reciprocal space, have been modeled with a Heisenberg Hamiltonian including isotropic exchanges up to the third nearest neighbors and a planar magnetic anisotropy. This yielded the exchange integral values J_1=−21.5 K, J_2=0.67 K, and J_3=−2.87 K. These results are presented and compared to experimental values of relevant diluted magnetic semiconductors, allowing a discussion on a generic description of the distance dependence of the nearest-neighbor magnetic interactions.

DOI: 10.1103/PhysRevB.73.104403 PACS number(s): 75.25.+z, 61.12.−q, 75.30.Ds, 75.50.Pp

I. INTRODUCTION

Magnetic semiconductors and semimagnetic (diluted magnetic) semiconductors (DMSs) have been extensively studied in the past, but recently, the possibility of applications in spin electronic devices has renewed the interest for this kind of materials, especially when they exhibit magnetic properties at room temperature. In this context, the knowledge of the magnetic characteristics of ferromagnetic or antiferromagetic semiconductors becomes important.

Among stable binary manganese compounds, MnTe is known as the only one that exhibits semiconductor properties. Most of such compounds are either metallic (e.g., MnAs or MnSb), or insulating (e.g., MnO or MnS). It has been established that MnTe in NiAs structure is a *p*-type semiconductor with a typical free-hole concentration $p=10^{18}$ cm^{-3} and an indirect energy gap close to E_g=1.27 eV at room temperature (see Refs. 1–3, and references therein). The particularity of MnTe as a crossroads material was first pointed out in Ref. 4 and more recently in Ref. 5. It has been demonstrated that, roughly speaking, this exceptional property is related to the energy positions of occupied and unoccupied Mn *d* states (resulting from the energy splitting of the 3*d* band) in the band structure of hexagonal MnTe. From one side, occupied *d* bands retain their narrow character and on the other side an extensive *p*-*d* overlap takes place with Te *p* bands forming the top of the valence band. This idea first proposed in Ref. 4 has been confirmed both by the band structure calculations,[6,5] and by photoemission and inverse photoemission direct measurements.[7,8]

Hexagonal MnTe, with the NiAs structure, shown in Fig. 1, was already extensively investigated in the sixties, but the difficulty in getting samples and its very antiferromagnetic nature, even though persisting above room temperature, kept it aside. Antiferromagnetic properties are now welcome in view of their possible use in selected spintronics devices (such as, e.g., spin valves). Furthermore, hexagonal MnTe and Mn-rich $Zn_{1-x}Mn_xTe$,[9–11] as well as the zinc-blende (ZB) phase MnTe,[12–15] may be grown by molecular beam epitaxy (MBE) and thus applied in layered structures for this purpose.

The antiferromagnetism of hexagonal MnTe at low temperature and its transition towards a paramagnetic state at $T_N \approx 310$ K has been evidenced by the observation of anomalies in the temperature dependence of the specific heat, magnetic susceptibility, electrical resistivity, thermoelectric power, thermal conductivity, as well as in the value of the lattice constant *c*. The magnetic order and anisotropy have been investigated by many authors.[16–20] The temperature dependence of the lattice parameter *c* led to the conclusion that the magnetic structure was an antiparallel stacking of (001) ferromagnetic planes[21] and magnetic anisotropy measurements[22] demonstrated that the spins lie in the (001) plane. This has been confirmed by magnetic susceptibility measurements,[20] and finally directly measured by elastic neutron scattering.[23,24] The spin orientation within the plane is thought to be along the Mn-Mn nearest-neighbor direction,[2] which implies three kinds of magnetic domains,

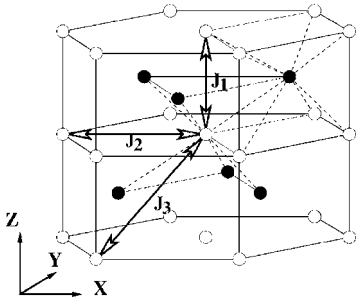

FIG. 1. The crystal lattice of MnTe in the hexagonal structure of NiAs type. Open circles correspond to Mn ions, full circles to Te ions. The double-arrowed lines illustrate the magnetic exchanges J_1, J_2, and J_3 between pairs of Mn ions, first, second, and third nearest neighbors, respectively.

but it could not be ascertained by experiments. The nuclear and magnetic structures are illustrated in Fig. 1 with the indications of the Mn-Mn magnetic exchanges up to the third magnetic neighbors.

As for II-VI-based diluted magnetic semiconductors[25–27] (DMSs) and ZB MnTe, the dominant mechanism responsible for the antiferromagnetism in hexagonal MnTe is the superexchange mediated by the Te anions, even though some authors suggested the possible contribution of a direct Mn -Mn exchange.[28] However, there is nearly no experimental information on the values of the relevant magnetic interactions. Some estimates have been proposed from indirect determination[1,29] but with so large discrepancies than none are actually reliable. A previous study of ZB MnTe[30,31] demonstrated the usefulness of spin-wave measurements to determine the magnetic exchange interactions.

So, to get a deeper insight into the magnetic properties of hexagonal MnTe, we have measured its spin-wave excitations at low temperature. From the data analysis with a model Hamiltonian, we could deduce the magnetic exchange interactions up to the third nearest neighbors and the dominant anisotropy.

The paper is organized as follows. In Sec. II the sample growth and characterization are presented. In Sec. III the spin-wave measurements are explained in detail and illustrated by several examples. In Sec. IV the data analysis is described and the results discussed.

II. SAMPLE GROWTH AND CHARACTERIZATION

One of the difficulties in obtaining high-quality samples of hexagonal MnTe is the existence of a $MnTe_2$ phase, often present as a contamination in bulk samples because of the necessity to start the growth with a Te-rich melt. Moreover, the easy oxidation of Mn, yielding a MnO contamination and increasing the $MnTe_2$ phase content in the ingot, requires that we strictly avoid oxygen at any step of the growth procedure.

The sample used for the neutron measurements has been grown in the Institute of Physics of the Polish Academy of Sciences in Warsaw from elements purified in this institute. A method of purification, particularly effective for removal of oxygen, carbon, and sulphur contaminations has been used in the case of Mn. The total contamination of our ultrapure manganese by other elements corresponded to the purity 6N, as that of Te. For the crystal growth we applied the physical vapour transport method, with materials closed in a silica ampoule with 9 mm inner radius and 2 mm thick wall. The obtained crystals were then annealed at 950 °C for several hours. The quality of single crystal grains was checked by x-ray diffraction on a high-resolution Philips X'Pert diffractometer. All features of the powder diffraction pattern, shown in Fig. 2, can be attributed to pure hexagonal MnTe within experimental accuracy, excluding the presence of any contamination by other phases or compounds. This yielded the lattice parameter values of $a=4.15$ Å and $c=6.71$ Å, in accordance with the values reported in the literature.[32]

A single crystal with a volume of about 30 mm^3 was selected for the neutron-scattering measurements. Neutron-diffraction measurements as a function of temperature[33] confirmed the lattice parameter values and allowed the determination of the magnetic moment of the Mn ions, found to be $4.76\pm0.1\mu_B$, in agreement with the $4.66\mu_B$ deduced from theoretical predictions.[5]

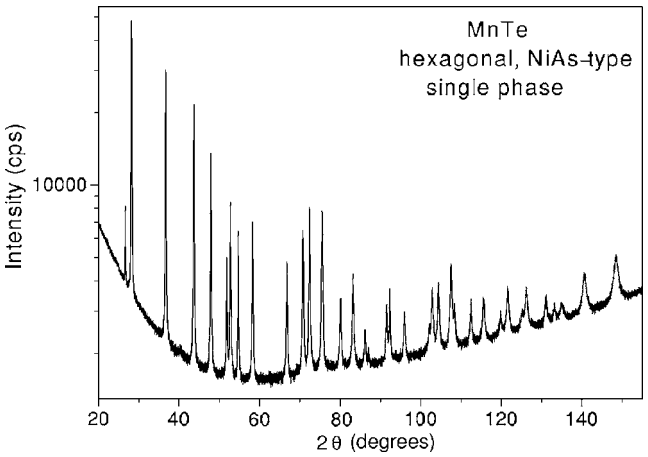

FIG. 2. Example of the x-ray diffraction pattern obtained with the use of high-resolution laboratory diffractometer and Cu $K\alpha_1$ radiation for hexagonal MnTe. All structures seen in a wide angular range (about 40 lines) are due to the diffraction on MnTe (no trace of precipitates has been found by this characterization method).

III. SPIN-WAVE MEASUREMENTS AND ANALYSIS

The magnetic unit cell of hexagonal MnTe is identical to the nuclear one and contains two Mn ions with spins oriented in opposite directions. Two spin-wave modes corresponding to a doubly degenerate acoustic mode are then expected in absence of any anisotropy. The existence of an easy-axis anisotropy should keep the degeneracy but open a gap at $q=0$, whereas the existence of an easy-plane anisotropy would remove the degeneracy and enhance the gap of one of the modes.

A. Experiments

The triple axis spectrometer 2T1 of the Orphée reactor of the Laboratoire Léon Brillouin (LLB) at Saclay was used for the inelastic neutron scattering measurements. All the measurements were carried out with a final neutron wave-vector $k_f=2.662$ $Å^{-1}$, with a graphite filter to prevent harmonics contamination. To get a maximum signal, no Soller slits collimation were used, the pyrolytic graphite monochromator, in 002 reflection (PG002), was vertically bent, and the PG002 analyzer was vertically and horizontally bent. The oriented sample was placed in a closed cycle refrigerator, measurements were performed at 11 ± 0.5 K. To collect as much pertinent data as possible, the sample was successively oriented in the scattering planes [100]-[001] and [110]-[001] to get access to symmetry directions involving several combinations of the reciprocal a^* and c^* axes, namely, [100], [001], [101], [110], and [111].

Each neutron group was analyzed to obtain the position, damping, and intensity of the spin-wave excitations. The

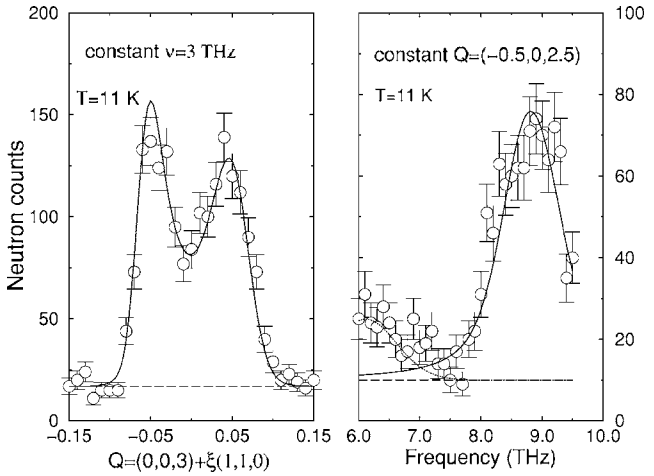

FIG. 3. Left panel: constant-frequency measurement in the [110] direction. Right panel: constant-Q measurement at the zone boundary in [110] direction, with a small contamination, likely a phonon, on the low-frequency side. The solid lines are the calculated lineshapes accounting for the experimental resolution, the dotted-dashed lines indicate the background level.

analysis accounted for the full geometry of the spectrometer, including monochromator and analyzer curvatures. After a first series of fits to obtain the overall shape of the mode dispersions, a second series of fits, accounting for the first and second derivatives of the dispersions, were achieved to get more precise results. Figure 3 displays two examples of measurement at constant frequency[34] and constant Q, with the line shapes resulting from the convolution of the fitted spin-wave dispersion with the experimental resolution. Figure 4 shows the gap observed at the Brillouin zone center (0,0,3). Due to the NiAs structure the signal at this position

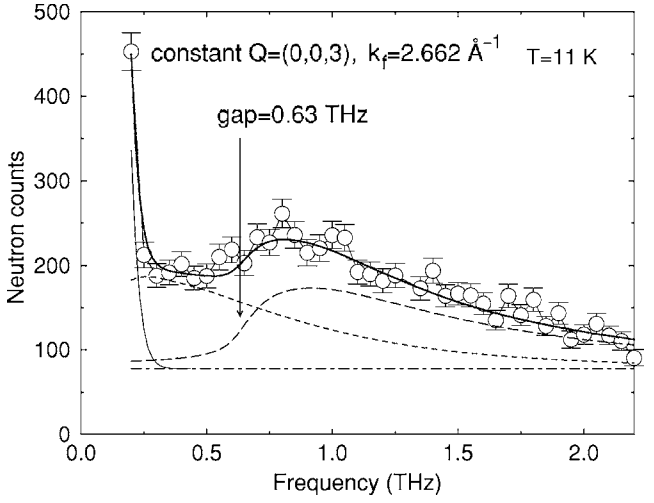

FIG. 4. Measurement at constant Q on the (003) antiferromagnetic Bragg peak position. Open symbols are the experimental values. The full line is the calculated lineshape, including a background (dotted-dashed line), a Bragg tail contamination (thin line), and two spin-wave contributions: one with a resolved gap (long-dashed line), the other with a nonresolved gap (dotted line).

is purely magnetic and the intensity still present below the gap points out the removal of the mode degeneracy associated with an easy-plane anisotropy.

B. Model Hamiltonian

The set of data ω versus q were used to adjust the values of the exchange integrals and anisotropy used to model the magnetic system via a Heisenberg Hamiltonian written as

$$\mathcal{H} = -\sum_{lm\lambda\mu} J_{lm\lambda\mu} \vec{S}_{l\lambda} \cdot \vec{S}_{m\mu} + \sum_{l\lambda} D S_{l\lambda}^{z\,2} - h_a \sum_{l\lambda_\uparrow\lambda_\downarrow} (S_{l\lambda_\uparrow}^{\zeta} - S_{l\lambda_\downarrow}^{\zeta}),$$

where l and m are cell indices, λ and μ site indices inside the cell, and $J_{lm\lambda\mu}$ are the isotropic exchange integrals. The anisotropy terms include an easy-plane term involving S^z, the spin component along the c direction, and an easy-axis term involving S^ζ, the longitudinal spin component.

Following the development presented in Appendix of Ref. 30 for ZB MnTe, reduced to two operators instead of four, the eigenvalues are obtained from the equation

$$\begin{vmatrix} A_{11}-\omega & A_{12} & d & 0 \\ -A_{12} & -A_{11}-\omega & 0 & -d \\ -d & 0 & -A_{11}-\omega & -A_{12} \\ 0 & d & A_{12} & A_{11}-\omega \end{vmatrix} = 0$$

with $A_{11}=2S\{-\Sigma_{\mathrm{AF}}\gamma_{\mathrm{AF}}(\mathbf{0})+\Sigma_F[\gamma_F(\mathbf{0})-\gamma_F(\mathbf{q})]\}+h_a+DS$, which can be written as $A_{11}=A_{11}^0+h_a+d$, $A_{12}=2S\Sigma_{\mathrm{AF}}\gamma_{\mathrm{AF}}(\mathbf{q})$, and $d=DS$. γ_{AF} and γ_F refer to the contributions between antiparallel and parallel moments, respectively. Each contribution is a summation on a set $\{m\}$ of nth neighbors, such as $\Sigma_{\{m\}}\exp[-i\mathbf{q}\cdot\mathbf{r}_n(m)]$.

The solutions may be obtained analytically, yielding $\omega^2=A_{11}^2-(A_{12}\pm d)^2$, which may be written as $\omega_1^2=(A_{11}^0+h_a+A_{12})(A_{11}^0+h_a-A_{12}+2d)$, $\omega_2^2=(A_{11}^0+h_a-A_{12})(A_{11}^0+h_a+A_{12}-2d)$.

We clearly see the different effects of the anisotropy contributions at $\mathbf{q}=\mathbf{0}$, where $A_{11}^0+A_{12}=0$: when $d=0$ the easy-axis contribution h_a does not remove the mode degeneracy but only add a gap at the origin, while, when $d\neq 0$, the easy-plane anisotropy removes the degeneracy, adding a gap on only one of the two modes.

Within this scheme, the choice is then to define the relevant set of magnetic neighbors, and therefrom the set of meaningful parameters to get a good description of the measured spin-wave modes. The minimum set is generally supposed to take into account J_1, J_2, and J_3, magnetic interactions between nearest, next-nearest, and next-next-nearest neighbors. As illustrated in Fig. 4, the gap corresponding to an easy-axis anisotropy could not be resolved by the experiment, so we only kept an easy-plane anisotropy contribution in our refinement.

In the fitting procedure, the uncertainties on the Q positions, deduced from constant-frequency measurements, have been converted in uncertainties on the frequency position with the use of the local tangent to the dispersion, as reported in Fig. 5. The best solution corresponds to the set $J_1=-0.449\pm0.006$ THz $(-21.5\pm0.3$ K), $J_2=0.014\pm0.001$ THz $(0.67\pm0.05$ K), $J_3=-0.060\pm0.001$ THz $(-2.87\pm0.04$ K),

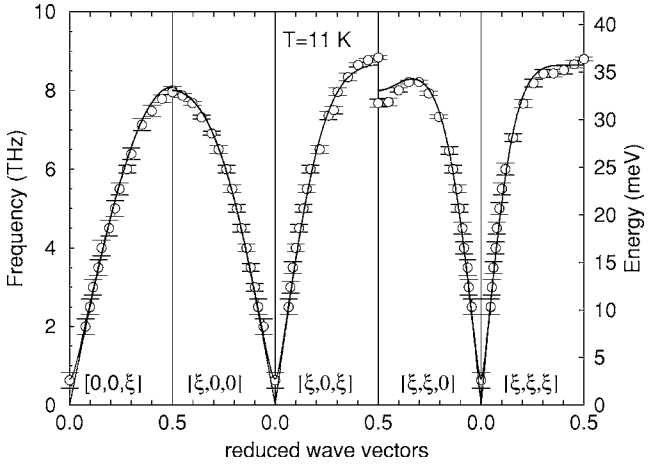

FIG. 5. Spin-wave dispersion measured in the five principal directions. Open symbols are the experimental values and full lines are the calculated dispersion using J_1, J_2, J_3, and D values, deduced from the fit to the model Hamiltonian.

and $D=-0.0054\pm0.0007$ THz $(-0.26\pm0.03$ K). The resulting calculated dispersions are plotted in Fig. 5, together with the experimental values.

Within the experimental accuracy, there is no obvious need for additional terms. Small discrepancies are seen near the zone boundaries, but they could be due to a small bias of the analysis associated with rapid changes in the dispersion curvatures.

IV. DISCUSSION

These results allow us to discard definitely the very few estimates previously done on the values of the exchange integrals in hexagonal MnTe. The first one[1] based on the relations between the exchange integrals and the values of T_N and Θ (paramagnetic Curie temperature), used a wrong assumption of the dominant interaction. The second one[29] used the results of a Raman scattering experiment which were analyzed with the assumption of a two-magnon contribution. The analysis, reduced to two adjustable parameters with the use of the molecular field approximation for T_N, yielded $J_1=-16.7$ K, $J_2=2.55$ K, and $J_3=-0.28$ K.

Actually our results point out the inadequacy of the relation $k_B T_N = 2S(S+1)/3(-2J_1+6J_2-12J_3)$, in the present case. This relation would yield $T_N \approx 475$ K with our experimental values, which means that the deviation from the molecular field approximation is indeed quite large in such a system.

At low temperature, the model Hamiltonian used to analyse our data provides a well defined set of exchange integrals, which allows a comparison with previous data from the literature.

A. Superexchange interactions with simple Mn-Mn bridge

In spite of many theoretical efforts there is no simple theory of the superexchange general enough to allow a direct quantitative comparison with our experimental results. This interaction is due to the overlap of the localized orbitals of the "magnetic" d-shell electrons with those of intermediate anions. From a phenomenological point of view, several factors are involved in the superexchange determination. First, for a given type of magnetic ion in a given crystal, the parameters describing the d-band splitting due to the lattice symmetry should be considered. Next, the type of interacting anion p and cation d orbitals (as well as the occupation state of the latter) has to be taken into account. In the case of perfect insulating systems the exchange mechanism may be described in real space, so that geometrical parameters, cation-cation distances, and cation-anion-cation bond angles are relevant. But, as soon as details of the band structure are implied, which is the case in semiconducting systems, corrections to the basic mechanism involve terms using a k-space description.

The geometrical description of the superexchange was first introduced by Anderson[35] and then developed by Goodenough[36,37] and Kanamori,[38] and improved again by Anderson.[39,40] The use of ligand field theory led to semiempirical rules, so-called Goodenough-Kanamori-Anderson (GKA) rules. Simple considerations on the orbitals fillings and the geometry of the orbitals overlapping allow predictions on the ferromagnetic or antiferromagnetic nature of the exchange and the order of magnitude of their ratio.

In the case of Mn^{2+}, a 180° superexchange (coupling two cations on opposite sides of an anion) is always antiferromagnetic. The sign of a 90° superexchange is not obvious. In particular, when the electron transfer between orbitals is not possible, weak ferromagnetism can be expected.

If we focus on "canonical" DMSs (II-VI compounds containing Mn), we find that the ZB cubic phase and the wurtzite (W) hexagonal phase involve superexchanges with simple cation-anion-cation bonds with similar bond angles of $\approx 109°$. Small deviations may appear because of structural distortion in the mixed crystals in ZB phases. For W-type compounds, distortions are also present depending on the c/a ratio and on the value of the u parameter defining the position of the pattern. Only for the ideal values $u=3/8$ and $c/a=\sqrt{8/3}$ the nearest-neighbor bonds have the same geometry as in the ZB structure. Nevertheless, the effects on the bond angles are small, of the order or ±1 degree, and only a small asymmetry exists on the cation-anion-cation bridges. Anyhow magnetization steps measurements on W-type diluted compounds provide two different values for in-plane and out-of-plane nearest-neighbor interactions (see the discussion in Ref. 41).

A large amount of experimental data has been accumulated on this DMS classes and especially on wide-gap DMSs, where geometrical considerations are expected to be dominant in the exchange determination. We have selected those obtained by experimental methods claimed to be the most accurate ones for this kind of problem.[42,43] We kept magnetization steps measurements on highly diluted systems and inelastic neutron scattering measurements either on highly diluted systems or on pure systems. Indeed with these methods the exchange integrals are obtained via solutions of a low-temperature Hamiltonian, without any assumption on sum rules linked to mean field models. We only kept one value, on HgMnS, deduced from magnetization and magnetic susceptibility measurements, for the comparison with

TABLE I. Experimental values of exchange interactions mediated by a single anion for group II–VI Mn-based DMSs and for two pure MnTe phases as a function of Mn-Mn distance. In the case of the wurtzite structure the two values correspond to two different nearest neighbors. Experimental methods: S=magnetization steps, N=inelastic neutron scattering, M=form of magnetization and magnetic susceptibility.

Compound	Mn-Mn (Å)	Interaction (K)	Method	Ref.
ZnMnO (W)	3.209	−18.2	S	44[a]
	3.25	−24.3	S	
	3.209	−17.7	N	59
	3.25	−23.5	N	
MnTe (NiAs)	3.345	−21.5	N	J_1[b]
ZnMnS (ZB)	3.83	−16.4	S	45
		−16.2	N	46
ZnMnSe (ZB)	4.00	−13.1	S	47
		−12.4	N	46
HgMnS (ZB)	4.13	−7.7	M	48
CdMnS (W)	4.14	−11.0	S	49
		−9.7	S	
CdMnSe (W)	4.30	−8.3	S	41
		−7.1	S	
HgMnSe (ZB)	4.30	−6.0	S	50
		−5.3	S	51
ZnMnTe (ZB)	4.31	−9.0	S	52
		−9.3	N	53[c]
MnTe(ZB)	4.48	−6.3	N	30
HgMnTe (ZB)	4.57	−5.1	S	50
		−4.3	S	51
CdMnTe (ZB)	4.58	−6.2	S	52
MnTe (NiAs)	5.315	−2.9	N	J_3[b]

[a]Maximum value attributed to the in-plane interaction, following Ref. 41.
[b]Present work.
[c]The original value given with better precision.

those deduced from magnetization steps measurements on HgMnSe and HgMnTe. This selection (with two values for magnetization steps measurements on W type compounds) is reported in Table I.

The values of J_1 and J_3 determined in the present study for MnTe in the NiAs hexagonal structure are also given in Table I. They both correspond to simple Mn-Te-Mn bridges, and we think that the comparison is meaningful in spite of their different bond angles. Indeed the bond-angle corresponding to J_1 is 71°, which means $90°-19°$, when the reference of the selection is $109°=90°+19°$. In the GKA approach the exchange is nearly symmetric around the 90° value which corresponds to its minimum, so we expect comparable values for bond angles of 71° and 109°.

In the case of J_3 the bond angle is ≈131°, and this higher value is expected to slightly enhance the exchange, which should evolve to a maximum at 180°. The values have been reported with linear-log and log-log scales in Fig. 6 and can be compared to an exponential law shown by the line in the upper panel of the figure or to a $1/R^{\alpha}$ law shown by the line in the lower panel. These lines have been obtained by fits to experimental values in the R range from 3.83 to 4.58 Å, using the higher values found by magnetization steps measurements and the values found by neutron measurements, with the exception of the mercury based compounds. Both approximations yield a fair agreement in this R range, but it is clear that such simple dependencies can not account for the evolution of the superexchange on the whole R range.

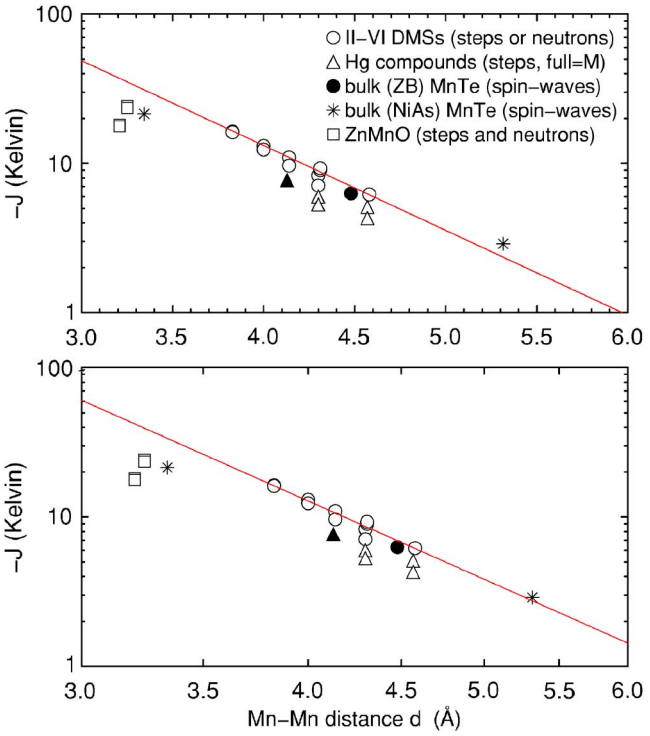

FIG. 6. (Color online) Experimental values of exchange interactions mediated by a single anion versus Mn-Mn distance d for selected semiconducting compounds with comparable bond angles, reported in Table I. Upper panel, linear-log plot, with a fit to an exponential law $J=J_0\exp(-AR)$, with $J_0=2.49\pm0.28\times10^3$ K and $A=1.31\pm.03$ Å^{-1}. Lower panel, log-log plot, with a fit to a law A/R^{α}, with $A=23.2\pm3.3\times10^3$ K and $\alpha=5.41\pm0.10$.

Whatever the law, there is obviously a leveling at lower R values. This trend has been recently backed up by neutron measurements[59] on ZnMnO, yielding J values in close agreement with those obtained by magnetization steps measurements.[44] This leveling points out a change in the R dependence which is likely related to more intricate effects taking place when R becomes small. This could be due to a saturation of the electron function overlap with decreasing R, and concomitant decreasing cation-anion distances, which would lead to a flat asymptotic behavior. But it could also be the signature of an increase of ferromagnetic contributions to the superexchange for small enough distances. Indeed, such contributions do exist,[40] even though they are supposed to be negligible in most cases, in the compounds relevant for our study.

We think that the behavior observed on a large scale of the Mn-Mn distance is significant and provides a realistic description of the dominant superexchange term in the case

of a simple cation-anion-cation bridging in Mn-based DMSs with a nearly constant bond angle. The lines drawn in Fig. 6 can be seen as "boundaries" of the R dependence of this interaction. The departures from these lines then point out peculiarities of the compounds related to their detailed electronic characteristics. The noticeable systematic discrepancy observed for the Hg-based mixed compounds could be an illustration of such an effect. Contrary to other DMSs of Table I, which are semiconductors with a wide energy gap, the mercury compounds are zero-gap materials (the conduction and valence bands are degenerated at the center of the Brillouin zone). The influence of the particular band structure of this group of materials on the magnetic properties has been previously suggested in Ref. 54. It should be also pointed out that a decrease of the superexchange interaction between the nearest neighbors with an increasing Mn-Mn distance for semiconductors, illustrated in Fig. 6, is much slower than that found for insulating metal oxides.[55]

The values corresponding to ZB and NiAs phase of pure MnTe are in perfect agreement with other data determined in highly diluted magnetic semiconductors. The experimental data for Mn-based mixed crystals containing different anions are distributed along the same line with a high accuracy which stresses the minor influence of the chemical character of the intermediating ion.

B. More distant exchange interactions

The case of more distant neighbors, with cations bridged by at least two anions, is far more intricate, as already pointed out by measurements on diluted systems and on pure ZB MnTe,[30] and the search for a simple phenomenological behavior would be hopeless. Only calculations accounting for detailed electronic properties, including conduction and valence bands, could give realistic estimates, as pointed out in Ref. 56 and recently performed[57] for exchange interactions between Mn ions in PbTe (rocksalt structure). Both experiments and calculations revealed indeed a nonmonotonous behavior.

If the values of J_1 and J_3 deduced from our measurements follow a standard behavior, the very small ferromagnetic value found for J_2 calls for some comments. As mentioned above, the 90° bond angle does not favor p-d hybridization. Moreover, the temperature dependence of the c parameter of hexagonal MnTe evidences an exchange striction along the c axis, which should result in a deformation of the orbitals, similarly to what has been observed in MnO by γ-ray diffraction measurements.[58] This still decreases the p-d functions overlap, and finally a weak ferromagnetic coupling due to the potential exchange becomes the dominant term, following the GKA rule.[39,40]

V. CONCLUSIONS

The spin-wave dispersion for MnTe with a NiAs hexagonal structure, measured by inelastic neutron scattering and modeled with a Heisenberg Hamiltonian, allowed the determination of isotropic exchange terms up to the third nearest neighbors and of an easy-plane anisotropy term. The values $J_1=-21.5$ K, $J_2=0.67$ K, $J_3-2.87$ K, and $D=-0.26$ K have been obtained. The J_2 value, corresponding to a 90° bond angle, is explained by the Goodenough-Kanamori-Anderson rule. It is the first clear observation of the ferromagnetic superexchange mediated by a single anion for semiconductor closely related to 3d-based DMSs. J_1 and J_3 values match very well with the trend of the distance dependence of the magnetic interaction, obtained from a selection of II-VI based DMSs with Mn having comparable bond angle.

These results, added to recent measurements on $Zn_{1-x}Mn_xO$,[44,59] provide a large increase of the range of Mn-Mn distances, where exchange integrals are known in the case of a single anion bridging with a given bond angle. This gives support to the existence of a generic behavior of the distance dependence of the nearest-neighbor superexchange in Mn-based DMSs. The departure from the generic line could give an estimate of the corrective term for compounds where the existence of more specific factors are expected to take place. We may hope that systematic departures will reveal the existence of subclasses more specific of the electronic characteristics of such systems.

ACKNOWLEDGMENTS

The authors would like to express their gratitude to A. Mycielski for his helpful advice concerning the details of the crystal growth and to E. Łusakowska for the x-ray analysis of the MnTe ingot by the Laue method. This work was supported in part by the Center of Excellence of the European Union CEPHEUS (Contract No. G1MA-CT-2002-04017), by the ACI NR0095 NANODYNE research project from the French Ministry of National Education, and by the research Grant No. PBZ/KBN/044/P03/2001 from the State Committee for Scientific Research (Poland). The experiments at LLB were supported by the European Commission through the Access Activities of the Integrated Infrastructure Initiative for Neutron Scattering and Muon Spectroscopy (NMI3) supported by the European Commission under the 6th Framework Programme through the Key Action: Strengthening the European Research Area, Research Infrastructures, Contract No. RII3-CT-2003-505925.

*Email address: szusz@ifpan.edu.pl

[1] G. Zanmarchi and C. Haas, Philips Res. Rep. **23**, 389 (1968).
[2] J. D. Wasscher, Philips Res. Rep., Suppl. (1969).
[3] Ch. Ferrer-Roca, A. Segura, C. Reig, and V. Munoz, Phys. Rev. B **61**, 13679 (2000).
[4] J. W. Allen, G. Lucovsky, and J. C. Mikkelsen, Jr., Solid State Commun. **24**, 367 (1977).
[5] S. J. Youn, B. I. Min, and A. J. Freeman, Phys. Status Solidi B **241**, 1411 (2004).
[6] S. H. Wei and A. Zunger, Phys. Rev. B **35**, 2340 (1987).

[7] H. Sato, M. Tamura, N. Happo, T. Mihara, M. Taniguchi, T. Mizokawa, A. Fujimori, and Y. Ueda, Solid State Commun. **92**, 921 (1994).
[8] H. Sato, T. Mihara, A. Furuta, M. Tamura, K. Mimura, N. Happo, M. Taniguchi, and Y. Ueda, Phys. Rev. B **56**, 7222 (1997).
[9] H. Akinaga and K. Ando, Mater. Sci. Forum **182-184**, 483 (1995).
[10] E. Dynowska and E. Przeździecka, J. Alloys Compd. **401**, 265 (2005).
[11] E. Przeździecka, E. Kaminska, E. Dynowska, E. Janik, R. Butkute, W. D. Dobrowolski, M. Sawicki, H. Kępa, R. Jakiela, M. Aleszkiewicz, and J. Kossut, Phys. Status Solidi C **2**, 1218 (2005).
[12] S. M. Durbin, J. Han Sungki, O. M. Kobayashi, D. R. Menke, R. L. Gunshor, Q. Fu, N. Pelenakos, A. V. Nurmikko, D. Li, J. Gosvales, and N. Otsuka, Appl. Phys. Lett. **55**, 2087 (1989).
[13] J. R. Buschert, F. C. Peiris, N. Samarth, H. Luo, and J. K. Furdyna, Phys. Rev. B **49**, 4619 (1994).
[14] H. Akinaga, K. Ando, T. Abe, and S. Yoshida, J. Appl. Phys. **74**, 746 (1993).
[15] E. Janik, E. Dynowska, J. Bak-Misiuk, M. Leszczynski, W. Szuszkiewicz, T. Wojtowicz, G. Karczewski, A. K. Zakrzewski, and J. Kossut, Thin Solid Films **267**, 74 (1995).
[16] E. Uchida, H. Kondoh, and N. Fukuoka, J. Phys. Soc. Jpn. **11**, 27 (1956).
[17] K. Adachi, J. Phys. Soc. Jpn. **16**, 2187 (1961).
[18] H. Yadaka, T. Harada, and E. Hirahara, J. Phys. Soc. Jpn. **17**, 875 (1961).
[19] J. J. Banewicz, R. F. Heidelberg, and A. H. Luxem, J. Phys. Chem. **65**, 615 (1961).
[20] T. Komatsubara, M. Murakami, and E. Hirahara, J. Phys. Soc. Jpn. **18**, 356 (1963).
[21] S. Greenwald, Acta Crystallogr. **6**, 396 (1953).
[22] K. Hirakawa, according to Kunitomi et al. (Ref. 23).
[23] N. Kunitomi, Y. Hamaguchi, and S. Anzai, J. Phys. Radium **25**, 568 (1964).
[24] N. N. Sirota and G. I. Makovetskii, Dokl. Akad. Nauk SSSR **170**, 1300 (1965) [Sov. Phys. Dokl. **11**, 888 (1967)]. See also relevant references (in Russian).
[25] J. Spałek, A. Lewicki, Z. Tarnawski, J. K. Furdyna, R. R. Gałazka, and Z. Obuszko, Phys. Rev. B **33**, 3407 (1986).
[26] A. Lewicki, J. Spałek, J. K. Furdyna, and R. R. Gałazka, Phys. Rev. B **37**, 1860 (1988).
[27] B. E. Larson, K. C. Hass, H. Ehrenreich, and A. E. Carlsson, Phys. Rev. B **37**, 4137 (1988).
[28] H. Sugiura, A. Sawaoka, and S. Saito, J. Phys. Chem. Solids **40**, 701 (1979).
[29] S. R. Mobasser and T. R. Hart, Proc. SPIE **524**, 137 (1985).
[30] B. Hennion, W. Szuszkiewicz, E. Dynowska, E. Janik, and T. Wojtowicz, Phys. Rev. B **66**, 224426 (2002).
[31] B. Hennion, W. Szuszkiewicz, E. Dynowska, E. Janik, and T. Wojtowicz, J. Supercond. **16**, 151 (2003).
[32] M. E. Schlesinger, J. Phase Equilib. **19**, 591 (1998).
[33] W. Szuszkiewicz, B. Hennion, B. Witkowska, E. Łusakowska, and A. Mycielski, Phys. Status Solidi C **2**, 1141 (2005).
[34] A frequency of 1 THz corresponds to a wave number of 33.33 cm^{-1}, an energy of 4.135 meV, or a temperature of 48 K.
[35] P. W. Anderson, Phys. Rev. **79**, 350 (1950).
[36] J. B. Goodenough, Phys. Rev. **100**, 564 (1955).
[37] J. B. Goodenough, J. Phys. Chem. Solids **6**, 287 (1958).
[38] J. Kanamori, J. Phys. Chem. Solids **10**, 87 (1959).
[39] P. W. Anderson, in *Solid State Physics*, edited by F. Seitz and D. Turnbull (Academic Press, New York 1963), Vol. 14, p. 99.
[40] P. W. Anderson, in *Magnetism*, edited by G. T. Rado and H. Suhl (Academic Press, New York 1963), Vol. 1, p. 25.
[41] V. Bindilatti, T. Q. Vu, Y. Shapira, C. C. Agosta, E. J. McNiff, Jr., R. Kershaw, K. Dwight, and A. Wold, Phys. Rev. B **45**, 5328 (1992).
[42] Y. Shapira and V. Bindilatti, J. Appl. Phys. **92**, 4155 (2002).
[43] W. Szuszkiewicz and E. Dynowska, J. Alloys Compd. **401**, 272 (2005).
[44] X. Gratens, V. Bindilatti, N. F. Oliveira, Jr., Y. Shapira, S. Foner, Z. Golacki, and T. E. Haas, Phys. Rev. B **69**, 125209 (2005).
[45] According to Ref. [89] in Y. Shapira and V. Bindilatti, J. Appl. Phys. **92**, 4155 (2002).
[46] T. M. Giebultowicz, J. J. Rhyne, J. K. Furdyna, and P. Kłosowski, J. Appl. Phys. **67**, 5096 (1987).
[47] T. Yasuhira, K. Uchida, Y. H. Matsuda, N. Miura, and A. Twardowski, J. Phys. Soc. Jpn. **68**, T3436 (1999).
[48] K. Dybko, W. Szuszkiewicz, F. Palacio, E. Dynowska, W. Paszkowicz, and B. Witkowska, J. Magn. Magn. Mater. **192**, 61 (1999).
[49] Y. Shapira, S. Foner, D. Heiman, P. A. Wolff, and C. R. McIntyre, Solid State Commun. **71**, 355 (1989).
[50] R. R. Galazka, W. Dobrowolski, J. P. Lascaray, M. Nawrocki, A. Bruno, J. M. Broto, and J. C. Ousset, J. Magn. Magn. Mater. **72**, 174 (1988).
[51] J. Lascaray, A. Bruno, J. C. Ousset, H. Rakoto, J. M. Broto, and S. Askenazy, Physica B **155**, 353 (1989).
[52] S. Foner, Y. Shapira, D. Heiman, P. Becla, R. Kershaw, K. Dwight, and A. Wold, Phys. Rev. B **39**, 11793 (1989).
[53] H. Kępa, V. K. Le, C. M. Brown, M. Sawicki, J. K. Furdyna, T. M. Giebultowicz, and T. Dietl, Phys. Rev. Lett. **91**, 087205 (2003).
[54] K. Dybko, W. Szuszkiewicz, E. Dynowska, and F. Palacio, Phys. Rev. B **68**, 092411 (2003).
[55] E. A. Harris, J. Phys. C **5**, 338 (1972).
[56] J. Ginter, J. Kossut, and L. Świerkowski, Phys. Status Solidi B **96**, 735 (1979).
[57] A. Łusakowski and M. Górska, Acta Phys. Pol. A **103**, 659 (2003).
[58] W. Jauch and M. Reehuis, Phys. Rev. B **67**, 184420 (2003).
[59] H. Kępa, S. Kolesnik, Z. Wiren, J. Leao, C. M. Brown, B. Dabrowski, J. K. Furdyna, and T. M. Giebultowicz, Physica B (to be published); S. Kolesnik, B. Dabrowski, Z. Q. Wiren, H. Kępa, T. M. Giebultowicz, C. M. Brown, J. Leao, and J. K. Furdyna, J. Appl. Phys. (to be published).